Interlayer interaction, shear vibrational mode, and tribological properties of two-dimensional bilayers with a commensurate moiré pattern

Alexander S. Minkin [1,*] Irina V. Lebedeva [2,†] Andrey M. Popov [3,‡] Sergey A. Vyrko [4,§] Nikolai A. Poklonski [4,‖] and Yurii E. Lozovik[3,5,¶]

[1]*Keldysh Institute of Applied Mathematics of Russian Academy of Sciences, 4 Miusskaya Square, Moscow 125047, Russia*
[2]*Simune Atomistics, Avenida de Tolosa 76, San Sebastian 20018, Spain*
[3]*Institute for Spectroscopy of Russian Academy of Sciences, Fizicheskaya Street 5, Troitsk, Moscow 108840, Russia*
[4]*Physics Department, Belarusian State University, Nezavisimosti Avenue 4, Minsk 220030, Belarus*
[5]*Moscow Institute of Electronics and Mathematics, National Research University Higher School of Economics, Bol'shoj Trekhsvjatitel'skij Pereulok 1-3/12, Building 8, Moscow 101000, Russia*

The potential energy surface (PES) of the interlayer interaction of infinite twisted bilayer graphene is calculated for a set of commensurate moiré patterns using the registry-dependent Kolmogorov-Crespi empirical potential. The calculated PESs have the same shape for all considered moiré patterns, and the unit cell size of the PESs is inversely related to the unit cell size of the moiré pattern. The amplitude of PES corrugations is found to decrease exponentially upon increasing the size of the moiré pattern unit cell. An analytical expression for such a PES including the first Fourier harmonics compatible with the symmetries of both layers is derived. It is shown that the calculated PESs can be approximated by the derived expression with an accuracy within 1%. This means that different physical properties associated with relative in-plane motion of graphene layers are interrelated and can be expressed analytically as functions of the amplitude of PES corrugations. In this way, we obtain the shear mode frequency, the shear modulus, the shear strength, and the barrier for relative rotation of the commensurate twisted layers to a fully incommensurate state for the considered moiré patterns. This barrier may possibly lead to robust macroscopic superlubricity for a twisted graphene bilayer with a commensurate moiré pattern. The conclusions drawn should be valid for diverse two-dimensional systems of twisted commensurate layers.

I. INTRODUCTION

Structural superlubricity, i.e., the mode of relative motion of the layers with vanishing or nearly vanishing friction [1,2], has attracted considerable attention in the context of discovery of graphene and other two-dimensional (2D) materials; see Ref. [3] for a review. First this phenomenon was observed for nanoscale contacts between graphene flakes at the tip of a microscope probe and a graphite surface [4–6]. A wide set of atomistic simulations has been devoted to superlubricity for 2D systems with a finite size of the contact area where the edge or rim contribution to the static friction is dominant [4,6–16]. Recently, not only nanoscale but also micro- and macroscale superlubricity has been found in systems of 2D layers [17–20]. These studies raise interest in possible factors which cause the static friction and can restrict superlubricity for a macroscale incommensurate contact area [3,8,18,21–23]. The following possible reasons of very low but nevertheless nonzero static friction have been considered: (1) the contribution of incomplete unit cells located at the rim area of one of the layers forming a moiré pattern (rim contribution) [8], (2) incomplete static friction force cancellation within complete unit cells of a commensurate moiré pattern (area contribution) [8], (3) the motion of domain walls of large commensurate domains formed upon relaxation of moiré patterns [3,18,21], and (4) the contribution of atomic-scale defects [18,22,23]. This paper is devoted to the detailed study of the area contribution to the static friction by the example of the twisted graphene bilayer.

Whereas for very small twist angles, the size of the moiré pattern unit cell is large [24] and, therefore, formation of commensurate domains separated by incommensurate domain boundaries occurs during the structural relaxation [25], for twist angles far from the coaligned orientation (0°, 60°, and so on), the size of the moiré pattern unit cell is smaller than or comparable to the width of commensurate domain walls (about 10 nm for bilayer graphene [26]). For such angles, relaxation to the commensurate domains is not possible, and a set of commensurate moiré patterns can be observed [24,27]. Twisted bilayer graphene with a commensurate moiré pattern has an interlayer interaction energy that is slightly lower than in a fully incommensurate state [7]. Thus one can expect that such patterns can be formed preferably for the corresponding range of twist angles. Here we propose that the energetic

*amink@mail.ru
†liv_ira@hotmail.com
‡popov-isan@mail.ru
§vyrko@bsu.by
‖Corresponding author: poklonski@bsu.by
¶lozovik@isan.troitsk.ru

preference of commensurate moiré patterns can also lead to the robust superlubricity. This is why the study of tribological properties of 2D systems with commensurate moiré patterns is of high interest.

The tribological properties are determined by the potential energy surface (PES) of the interlayer interaction, that is, the dependence of this energy on coordinates describing the relative in-plane displacement of 2D layers. Previous atomistic calculations allowed the area contribution to the static friction of the twisted graphene bilayer to be distinguished for a few commensurate moiré patterns [7,8,28]. Cancellation of the static friction force within complete unit cells of commensurate moiré patterns of a graphene bilayer [8,22,23] and double-walled carbon nanotubes [29–31] has been also demonstrated. However, the symmetry and shape of the PES of the interlayer interaction for commensurate moiré patterns of infinite twisted graphene bilayers has not been studied yet. Recently, we proposed a hypothesis that such PESs in diverse 2D materials with layers aligned in the same or opposite directions can be universally described by the first spatial Fourier harmonics [32]. This hypothesis has been confirmed by calculations of PESs for different 2D materials [32–39] and 2D heterostructures [40–43]. Moreover, this hypothesis is valid also for double-walled carbon nanotubes [30,44–48], where only Fourier harmonics compatible with the symmetry of both walls contribute to the PES of the interwall interaction [44,47]. By analogy with double-walled nanotubes, one might expect that the PES for the interlayer interaction of twisted layers of an infinite commensurate moiré pattern is determined by Fourier harmonics compatible with the symmetries of both layers, i.e., with the symmetry of the whole moiré pattern. In such a case, the approximated PES depends on a single parameter, and the set of physical quantities determined by the PES are interrelated [35,39].

Here we calculate the PESs for a wide set of infinite commensurate moiré patterns of twisted graphene bilayers using the registry-dependent Kolmogorov-Crespi potential [49] and show that these PESs can be excellently approximated by the first Fourier harmonics which are compatible with the symmetry of the whole moiré pattern. The PES approximation derived is used to obtain analytical expressions for a set of physical quantities of moiré patterns determined by the PES such as the shear frequency, the shear modulus, the shear strength, and the barrier for relative rotation of the layers to a fully incommensurate state.

The paper is organized in the following way. In Sec. II, the model of the superlubric system and the calculation methods are described. Section III is devoted to our results from the PES calculations and approximations by Fourier harmonics as well as estimates of physical quantities determined by the PES. The conclusions and a discussion are presented in Sec. IV.

II. METHODOLOGY

A. Structure of the commensurate twisted graphene bilayer

Let us consider first the structure of the commensurate twisted graphene bilayer. The commensurate moiré pattern (n_1, n_2) is defined by the indices n_1 and n_2, which are coprime numbers [27]. It has been shown that for each moiré pattern

(n_1, n_2), there is a twin pattern (n'_1, n'_2) with greater indices n'_1 and n'_2 with the same size of the unit cell [24,27]. In the pairs of indices of twin moiré patterns, $(n_1 - n_2)/3$ is not an integer for the smaller pair of indices, whereas $(n'_1 - n'_2)/3$ is an integer for the greater indices. Examples of twin commensurate moiré patterns are shown in Fig. 1.

If $(n_1 - n_2)/3$ is not an integer, the unit cell of the commensurate moiré pattern (n_1, n_2) is defined by lattice vectors $\mathbf{L}_1$ and $\mathbf{L}_2$ [see Fig. 1(a)]

$$\mathbf{L}_1 = n_1\mathbf{a}_1 + n_2\mathbf{a}_2, \quad \mathbf{L}_2 = -n_2\mathbf{a}_1 + (n_1 + n_2)\mathbf{a}_2,$$

where $\mathbf{a}_1$ and $\mathbf{a}_2$ are lattice vectors of the bottom graphene layer.

If $(n'_1 - n'_2)/3$ is an integer, the same equations give the vectors, one of which corresponds to the diagonal of the moiré pattern unit cell [see Fig. 1(b)]

$$\mathbf{L}'_1 = n'_1\mathbf{a}_1 + n'_2\mathbf{a}_2, \quad \mathbf{L}'_2 = -n'_2\mathbf{a}_1 + (n'_1 + n'_2)\mathbf{a}_2.$$

In this case the indices n_1 and n_2 which determine the moiré pattern unit cell

$$\mathbf{L}_1^{(u)} = n_1\mathbf{a}_2 + n_2\mathbf{a}_1, \quad \mathbf{L}_2^{(u)} = -n_2\mathbf{a}_2 + (n_1 + n_2)\mathbf{a}_1$$

for given n'_1 and n'_2 can be found from any of the equations

$$\mathbf{L}'_1 = \mathbf{L}_1^{(u)} + \mathbf{L}_2^{(u)}, \quad \mathbf{L}'_2 = 2\mathbf{L}_1^{(u)} - \mathbf{L}_2^{(u)}$$

in the form

$$n_1 = \frac{n'_1 + 2n'_2}{3}, \quad n_2 = \frac{n'_1 - n'_2}{3}.$$

The angle θ of relative rotation of graphene layers of the commensurate moiré pattern (that is, the angle between the vectors $\mathbf{a}_1$ and $\mathbf{a}'_1$) is defined as

$$\cos\theta = \frac{n_1^2 + 4n_1n_2 + n_2^2}{2(n_1^2 + n_1n_2 + n_2^2)}.$$

In the case where $(n_1 - n_2)/3$ is not an integer, the angle φ between the lattice vector $\mathbf{a}_1$ and the lattice vector of commensurate moiré pattern $\mathbf{L}_1 = n_1\mathbf{a}_1 + n_2\mathbf{a}_2$ is

$$\varphi = 30° - \frac{\theta}{2}.$$

The area of the unit cell of moiré pattern (n_1, n_2) is

$$S = S_g N_c = \frac{\sqrt{3}a^2(n_1^2 + n_1n_2 + n_2^2)}{2R},$$

where $S_g = \sqrt{3}a^2/2$ is the area of the unit cell of graphene, $a = |\mathbf{a}_1| = |\mathbf{a}_2|$ is the graphene lattice constant, and $N_c = (n_1^2 + n_1n_2 + n_2^2)/R$ is the number of unit cells of graphene per unit cell of the commensurate moiré pattern; the parameter $R = 3$ if $(n_1 - n_2)/3$ is an integer, and $R = 1$ otherwise.

Pairs of twin commensurate moiré patterns with the same size of the unit cell and with different symmetry of the stacking just after the relative rotation of layers were considered as different in the original work by Mele [27]. However, one commensurate moiré pattern in such a pair can be obtained from the other by the translational displacement $\mathbf{t}$ of one of the layers in the layer plane (see Fig. 1). Here we study the PES of the interlayer interaction energy as a function of the coordinates describing the in-plane relative displacement of
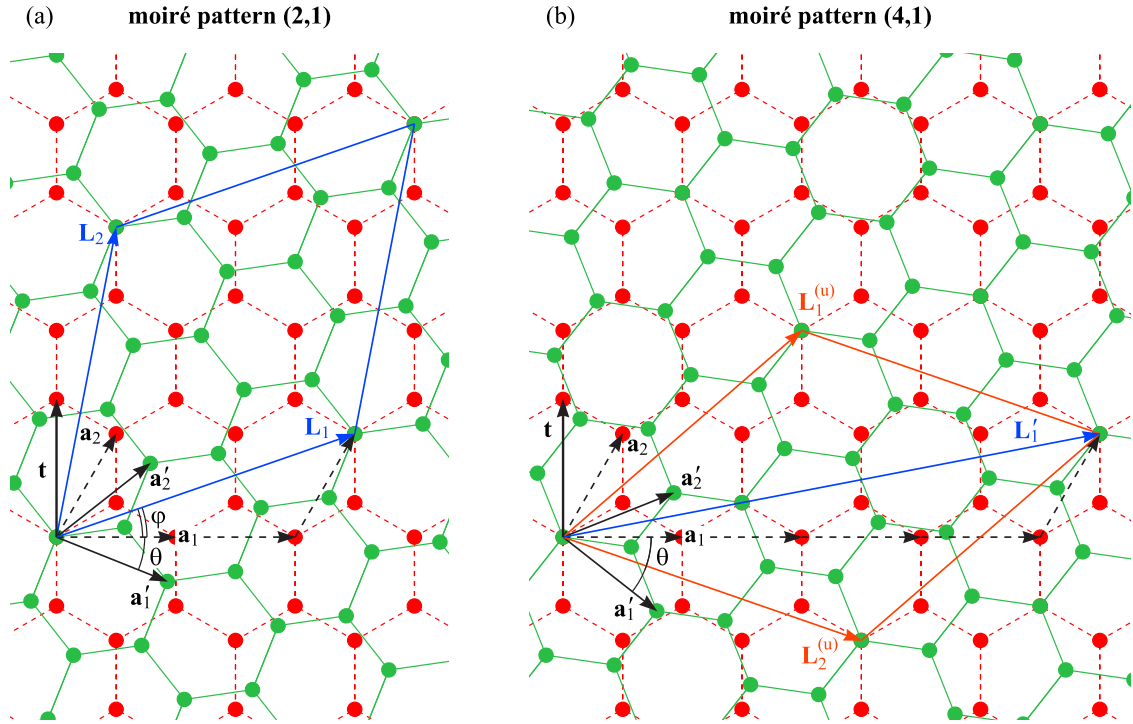
FIG. 1. (a) and (b) Schemes of twin commensurate moiré patterns (2,1) and (4,1) of a twisted graphene bilayer, respectively, with the same size of the unit cell. Lattice vectors $\mathbf{a}_1$ and $\mathbf{a}_2$ of the bottom graphene layer and $\mathbf{a}'_1$ and $\mathbf{a}'_2$ of the top layer, lattice vectors $\mathbf{L}_1$ and $\mathbf{L}_2$ of the commensurate moiré pattern, angle θ of relative rotation of the graphene layers, and angle φ between the lattice vector $\mathbf{a}_1$ of the bottom layer and the lattice vector of commensurate moiré pattern $\mathbf{L}_1$ are indicated. The translational displacement $\mathbf{t}$ of the upper layer that converts one moiré pattern into the other is shown by thick black arrows.

the layers. Evidently, the moiré patterns related by the translational displacement $\mathbf{t}$ correspond to the same PES. Thus only one pair of moiré patterns with the indices n_1 and n_2, where $(n_1 - n_2)/3$ is not an integer, are considered here for the PES calculations.

B. Computational details

The ratio of the PES corrugations to the average interlayer interaction energy is extremely small for twisted graphene bilayers [7,8,23]. Simultaneously, the size of the simulation cell and the number of computational runs for each considered moiré pattern are too high to study the PES of the interlayer interaction by *ab initio* methods. Thus we use classical potentials in this paper. At this moment, there are no experimental data on physical properties of systems of twisted layers that can be used to fit parameters of classical potentials for description of the interlayer interaction (or check the adequacy of existing potentials for twisted layers). The parameters of the popular Kolmogorov-Crespi and Lebedeva potentials (Tables S1 and S2 of the Supplemental Material [50]) for the interaction between graphene layers were fitted to the PES of the interlayer interaction of coaligned layers (with zero twist angle) obtained by density functional theory (DFT) calculations [34,49]. In the case of the Lebedeva potential, the experimental data on the frequency of in-plane interlayer vibrations of coaligned layers were also taken into account [35]. Nevertheless, corrugations of the PES computed for infinite commensurate moiré patterns using the Lebedeva potential do not exceed the calculation accuracy [22,23]. At the same time, they are finite and well defined for

commensurate moiré patterns with the smallest unit cells when the Kolmogorov-Crespi potential is used [7,8,23]. The explanation of this discrepancy between the Kolmogorov-Crespi and Lebedeva potentials is discussed in Sec. III B. In this paper, all calculations are performed using the Kolmogorov-Crespi potential, which allows us to analyze the shape of the PES determined by the symmetry of the commensurate twisted graphene bilayer. However, we emphasize that the results obtained here are only of qualitative nature.

The PES calculations have been carried out under periodic boundary conditions. Simulation cells of height 100 Å have been used for all the considered moiré patterns. The bond length between atoms in the graphene layers is taken to be equal to 1.42 Å. The upper graphene layer is placed at the interlayer distance of 3.46 Å [which is determined here on the example of the (2,1) moiré pattern to be optimal for the Kolmogorov-Crespi potential] and is rigidly shifted with respect to the bottom layer with steps of 0.0168 and 0.0193 Å in the zigzag and armchair directions of the bottom layer, respectively. Further calculation details which are different for eight considered moiré patterns with the smallest sizes of the unit cell are listed in Table I.

III. RESULTS

A. PES of the twisted graphene bilayer

The amplitude ΔU of PES corrugation (i.e., the difference between maximum and minimum values of the interlayer interaction energy, $\Delta U = U_{\max} - U_{\min}$) exceeds the calculation accuracy only for five out of eight considered moiré patterns

TABLE I. Calculation details for the considered commensurate moiré patterns with coprime indices (n_1, n_2): the angle θ of relative rotation of graphene layers, the number of atoms N_c in the moiré pattern unit cell, the simulation cell size in the units of moiré pattern unit cells, the total number of atoms N_a in the simulation cell, and the cutoff radius R_c of the Kolmogorov–Crespi potential.

(n_1, n_2)	θ (deg)	N_c	Cell size	N_a	R_c (Å)
(2,1)	21.787	7	18 × 18	9072	16
(3,1)	32.204	13	18 × 18	16848	16
(3,2)	13.174	19	10 × 10	7600	16
(5,1)	42.103	31	11 × 11	15004	70
(5,3)	16.426	49	9 × 9	15876	70
(7,2)	35.567	67	6 × 6	9648	50
(7,3)	26.008	79	6 × 6	11376	50
(7,5)	10.993	109	5 × 5	10900	50

with smaller sizes of the unit cells. Calculated PESs for these moiré patterns are shown in Fig. 2. For three out of eight considered moiré patterns with larger sizes of the unit cells (equivalent to the smaller sizes of the unit cells of the PES as shown below), the amplitude of PES corrugations is lower than the artifacts related with the finite value of the cutoff radius of the potential. Calculated PESs for these moiré patterns are shown in Fig. S1 of the Supplemental Material [50].

Two types of PESs have been found. The PESs of the first type have a triangular lattice of minima and a honeycomb lattice of maxima, whereas the PESs of the second type, in

contrast, have a triangular lattice of maxima and a honeycomb lattice of minima. As discussed in Sec. III B, the PES shape is described for both PES types by the same expression which contains only the first spatial Fourier harmonics and, therefore, only a single energetic parameter. The difference between the two types of PESs is determined by the sign of this parameter.

It should be noted that the number of unit cells of the PES per unit cell of graphene is the same as the number N_c of unit cells of graphene per unit cell of the moiré pattern (see also Sec. III B). The dependence of the amplitude ΔU of PES corrugations on the number N_c is shown in Fig. 2(f). The amplitude ΔU decreases nearly exponentially with the decrease in the size of the unit cell of the PES or, equivalently, with the increase in the size of the unit cell of the moiré pattern. The analogous exponential decrease in the amplitude of PES corrugations with the increase in the size of the unit cell of the moiré pattern was observed previously for rigid finite graphene layers [7] where the rim contribution to static friction is dominant. Note that the extremely low values of the amplitude ΔU for the moiré patterns with the smaller sizes of the PES unit cell make evident the necessity of using classical potentials for the PES calculations.

B. Approximation of the PES by the first Fourier harmonics

PESs of the interlayer interaction in diverse hexagonal 2D materials can be closely approximated by the expressions containing only the first spatial Fourier harmonics determined by the system symmetry. The adequacy of such an
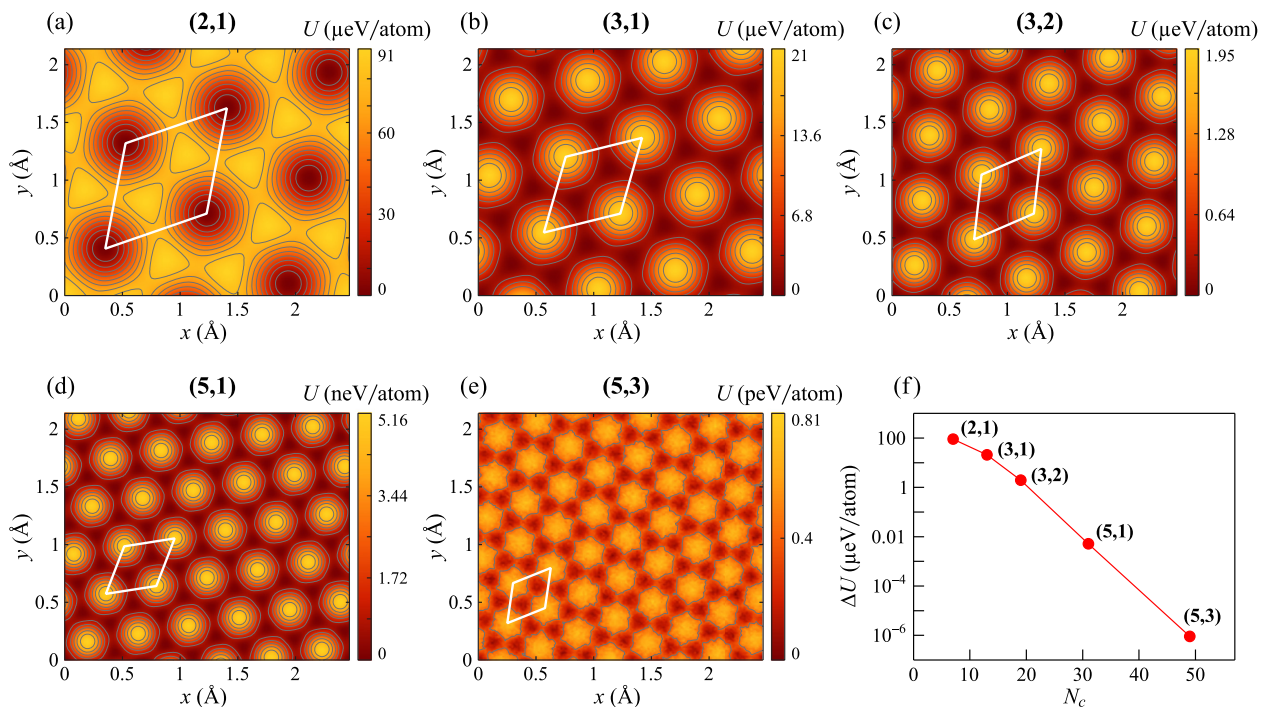

FIG. 2. (a)–(e) Potential energy U (per atom of the upper layer) of the interlayer interaction of a twisted graphene bilayer as a function of the relative displacement of the layers in the zigzag (x, in angstroms) and armchair (y, in angstroms) directions of the lower layer computed at the optimal interlayer distance of 3.46 Å for commensurate moiré patterns with coprime indices (a) (2,1), (b) (3,1), (c) (3,2), (d) (5,1), and (e) (5,3). The energy is given relative to the minimum. (f) Amplitude of PES corrugations, ΔU (per atom of the upper layer), as a function of the number N_c of unit cells of the PES per unit cell of graphene. The indices of the considered moiré patterns are indicated.
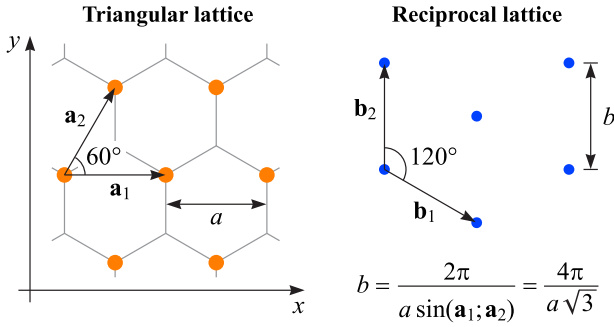
FIG. 3. Triangular lattice (orange dots) and its reciprocal lattice (blue dots). The lattice vectors $\mathbf{a}_1$ and $\mathbf{a}_2$ ($|\mathbf{a}_1| = |\mathbf{a}_2| = a$) as well as the reciprocal lattice vectors $\mathbf{b}_1$ and $\mathbf{b}_2$ are shown. The graphene honeycomb lattice is shown with gray lines. Coordinate x corresponds to the zigzag direction of the graphene layer.

approximation was demonstrated for coaligned graphene layers [33–35,37,38], hexagonal boron nitride (h-BN) [37,39], hydrofluorinated graphene [32], a graphene/h-BN heterostructure [41–43], and double-layer graphene with a krypton spacer [40].

These approximations are based on the following considerations. The translational symmetry of the PES for an atom adsorbed on a triangular lattice is the same as the translational symmetry of the triangular lattice; that is, $U_a(\mathbf{r}) = U_a(\mathbf{r} + n_1\mathbf{a}_1 + n_2\mathbf{a}_1)$, where $\mathbf{a}_1$ and $\mathbf{a}_2$ are the lattice vectors ($|\mathbf{a}_1| = |\mathbf{a}_2| = a$, and the angle between the vectors is 60°; Fig. 3), for any integer n_1 and n_2. This means that the Fourier transform of $U_a(\mathbf{r})$ consists of harmonics corresponding to vertices of the reciprocal lattice with the lattice vectors $\mathbf{b}_1$ and $\mathbf{b}_2$ such that $\mathbf{a}_i \cdot \mathbf{b}_j = 2\pi\delta_{ij}$ ($|\mathbf{b}_1| = |\mathbf{b}_2| = 4\pi/\sqrt{3}a$, and the angle between these vectors is 120°; Fig. 3). Taking into account only the first Fourier harmonics with wave vectors $\mathbf{b}_1$, $\mathbf{b}_2$ and $\mathbf{b}_1 + \mathbf{b}_2$, the PES for an atom on a triangular lattice can be approximated as

$$\delta U_a(\mathbf{r}) = U_{a,1}\text{Re}\left[e^{i\mathbf{b}_1\mathbf{r}} + e^{i\mathbf{b}_2\mathbf{r}} + e^{i(\mathbf{b}_1+\mathbf{b}_2)\mathbf{r}}\right], \quad (1)$$

where δU_a is the deviation from the average interaction energy between the atom and the lattice; point $\mathbf{r} = 0$ corresponds to the case when the atom is located on top of one of the lattice atoms.

For x and y axes chosen along one of the lattice vectors ($\mathbf{a}_1$) and in the perpendicular direction [4],

$$\delta U_a(x, y) = U_{a,1}[2\cos(k_y y)\cos(k_x x) + \cos(2k_y y)], \quad (2)$$

where $k_x = 2\pi/a$ and $k_y = 2\pi/\sqrt{3}a$.

To get the potential energy of an atom on a honeycomb lattice, it is necessary to sum up the expressions for two sublattices separated by $a/\sqrt{3}$ along the y axis (in the armchair direction). This leads to a sign change for the second term of Eq. (2). For two coaligned honeycomb layers, it is necessary to sum up once more the contributions of two sublattices of the adsorbed layer. This leads to another sign change in the equation. Thus the PES of coaligned honeycomb layers is described by an equation similar to Eq. (2) [33–35].

Now let us consider twisted honeycomb lattices. Let $\mathbf{a}_1$ and $\mathbf{a}_2$ be the lattice vectors of the bottom layer and $\mathbf{a}'_1$ and $\mathbf{a}'_2$ be the lattice vectors of the upper one. The PES of

twisted honeycomb lattices is periodic with respect to translation along any of these lattice vectors: $U(\mathbf{r}) = U(\mathbf{r} + n_1\mathbf{a}_1 + n_2\mathbf{a}_2) = U(\mathbf{r} + n'_1\mathbf{a}'_1 + n'_2\mathbf{a}'_2)$, where n_1, n_2, n'_1, and n'_2 are any integer numbers. Thus the harmonics that contribute to the Fourier transform of the PES of twisted honeycomb lattices should comply with the condition $\mathbf{G} = m_1\mathbf{b}_1 + m_2\mathbf{b}_2 = m'_1\mathbf{b}'_1 + m'_2\mathbf{b}'_2$, where $\mathbf{b}_1$ and $\mathbf{b}_2$ are the lattice vectors of the reciprocal lattice of the bottom layer, $\mathbf{b}'_1$ and $\mathbf{b}'_2$ are the lattice vectors of the reciprocal lattice of the upper one, and m_1, m_2, m'_1 and m'_2 are some integer numbers. This means that these Fourier harmonics correspond to overlapping vertices of the reciprocal lattices of the twisted layers. The reciprocal lattices of the twisted honeycomb layers are also two twisted honeycomb lattices forming a commensurate moiré pattern similar to one in real space. Therefore the first Fourier terms contributing to the PES in this case correspond to the lattice vectors of this moiré pattern of the reciprocal lattices. They have length $B = bL/a$, where L is the period of the moiré pattern, and are rotated with respect to the reciprocal lattice vectors by the same angle φ as the moiré pattern vectors are rotated with respect to the lattice vectors in real space. As a result, the PES of twisted honeycomb layers can be approximated in the same form as Eq. (2) if we consider the x' and y' axes to be aligned along one of the moiré pattern vectors and in the perpendicular direction as well as increase the wave vectors by a factor of $L/a = \sqrt{N_c}$:

$$\delta U(x', y') = U_1(2\cos(k'_y y')\cos(k'_x x') + \cos(2k'_y y')), \quad (3)$$

where $\delta U = U - U_{av}$ is the deviation from the average PES energy $U_{av} = \text{const}$, $x' = x\cos\varphi - y\sin\varphi$, $y' = y\cos\varphi + x\sin\varphi$, $k'_x = \sqrt{N_c}k_x$, and $k'_y = \sqrt{N_c}k_y$. Thus the PES of the interlayer interaction of an infinite graphene bilayer with a commensurate moiré pattern has the same shape as the PES for a graphene bilayer with coaligned layers (presented in Refs. [33–35,38]) and differs only by the PES amplitude and the period, which is lower by a factor of $\sqrt{N_c}$.

The derived equation (3) is used here for the approximation of the calculated PESs. To fit the amplitude ΔU of PES corrugations, the *single* parameter of the approximation is chosen as $U_1 = 2\Delta U/9$. The relative deviation ϵ of the approximated and computed PESs is found as the root-mean-square deviation divided by ΔU. As can be seen in Table II, this relative deviation varies from 0.02% to a maximum of 1% for all the considered moiré patterns. The relative deviations in previous studies of PESs of coaligned layers are about 1% for graphene [34,35], 0.1–0.3% for h-BN [39], 0.3% for a graphene/h-BN heterostructure [43], and 3% for hydrofluorinated graphene [32]. We believe that the simple shape of the PES obtained here is a universal property of commensurate twisted bilayers consisting of various 2D materials analogous to that of coaligned commensurate bilayers.

It should be noted that for coaligned graphene layers, $U_{a,1}$ in Eq. (2) is positive and corresponds to the repulsion between the atoms of the upper and lower layers [33–35,37,38]. In the case of a moiré pattern, the PES is determined by the sum of contributions from many atoms within the moiré pattern unit cell, and U_1 in Eq. (3) can be positive or negative (Fig. 2 and Fig. S1 of the Supplemental Material [50]) depending on at which symmetry points there is more repulsion between the layers.

TABLE II. Approximation parameters U_1, relative root-mean-square deviations ϵ, shear mode frequencies f, shear moduli C_{44}, shear strengths τ, and barriers ΔU_{rot} for relative rotation of the commensurate twisted layers to an incommensurate state estimated for different moiré patterns based on calculations with the Kolmogorov-Crespi potential.

Moiré pattern	U_1 (eV/atom[a])	ϵ	f (cm^{-1})	C_{44} (Pa)	τ (Pa)	ΔU_{rot} (eV/atom[a])
(2,1)	-2.02×10^{-5}	1.04×10^{-2}	9.153	3.91×10^{8}	1.67×10^{7}	6.07×10^{-5}
(3,1)	4.66×10^{-6}	5.34×10^{-3}	4.233	8.37×10^{7}	1.12×10^{6}	6.99×10^{-6}
(3,2)	4.34×10^{-7}	3.33×10^{-3}	1.561	1.14×10^{7}	1.26×10^{5}	6.50×10^{-7}
(5,1)	1.15×10^{-9}	2.04×10^{-3}	0.103	4.91×10^{4}	4.25×10^{2}	1.72×10^{-9}

[a]Per atom of the upper layer.

Let us discuss the discrepancy of the PESs obtained here using the Kolmogorov-Crespi potential and the results of the calculations using the Lebedeva potential, where no corrugations which exceed the calculation accuracy are observed for the (2,1) moiré pattern [22,23]. The PES of the interlayer interaction for coaligned graphene layers obtained by dispersion-corrected DFT (DFT-D) calculations is excellently approximated by the first Fourier harmonics [33–35,38]. The Lebedeva potential was specifically designed to reproduce this property of the PES, so that the relative root-mean-square deviation of the approximated and computed PESs is within several percent for the Lebedeva potential. A similar deviation for the Kolmogorov-Crespi potential is 20 times greater [34]. The greater deviation of the Kolmogorov-Crespi potential is related to the considerably larger amplitudes of Fourier harmonics other than the first ones (which exactly reproduce the approximated PES) including those compatible with the symmetry of commensurate twisted graphene bilayers and therefore responsible for the shape of corresponding PESs. This explains the discrepancy of the results obtained using the Kolmogorov-Crespi and Lebedeva potentials.

Equations (2) and (3) are derived based on the system symmetry and make sense not only for the interlayer interaction energy but also for other properties of 2D materials. For example, Eq. (2) was used to approximate the interlayer tunneling contribution to the Hamiltonian of graphene layers in Ref. [51]. Considering the Brillouin zone for twisted layers, the authors derived for them the explicit Hamiltonian and analyzed their band structures. A similar study was also performed for a graphene/h-BN heterostructure [41,51]. The use of Eq. (3) taking into account the symmetry of commensurate twisted bilayers might be considered to further simplify such models.

C. Properties related to the PES

A number of physical properties associated with the relative in-plane motion of the layers are determined by the PES at a constant interlayer distance [32,35,39,43]. Since the PES is described by a simple expression involving just one energetic parameter [see Eq. (3)], all these properties can be described analytically as functions of this parameter. Below, we use the PES for the considered moiré patterns to estimate the shear mode frequency, the shear modulus, the shear strength, and the barrier for relative rotation of the commensurate twisted layers to an incommensurate state.

The frequency of the shear mode E_{2g}, in which adjacent layers slide rigidly in the opposite in-plane directions, can be found from the PES curvature in a given energy minimum [32,35,39,43] as

$$f = \frac{1}{2\pi}\sqrt{\frac{1}{\mu}\frac{\partial^2 U}{\partial x'^2}} = \frac{1}{a}\sqrt{\frac{1}{\mu}U_{\text{eff}}}, \tag{4}$$

where $U_{\text{eff}} = (a/2\pi)^2 \partial^2 U/\partial x'^2$ is the second-order derivative of the energy per carbon atom of the upper layer in energy units and μ is the reduced mass. The latter for bilayer graphene is calculated as $\mu = m_{\text{C}}/2$, where m_{C} is the mass of a carbon atom.

From Eq. (3), it follows that the PES curvature corresponds to $U_{\text{eff}} = N_c U_1 = (2/9)N_c\Delta U$ for moiré patterns with $U_1 > 0$ and $-2N_c U_1$ for $U_1 < 0$. The shear mode frequencies estimated for different moiré patterns using the values of the parameter U_1 derived from the calculations with the Kolmogorov-Crespi potential are listed in Table II. They all are within 10 cm^{-1} and are considerably smaller than the shear mode frequency for the coaligned graphene layers: 35 cm^{-1} [34,36] and 21–34 cm^{-1} [52] according to DFT calculations and 28 ± 3 cm^{-1} [53] and 32 cm^{-1} [54] according to experiments. Indeed, as follows from Eq. (4), the frequency depends on the square root $\sqrt{\Delta U N_c}$ of the product of the amplitude ΔU of PES corrugations and the number N_c of unit cells of graphene per unit cell of the commensurate moiré pattern. Since ΔU decreases exponentially with the growth of N_c [Fig. 2(f)], the shear mode frequency also gets reduced upon increasing N_c.

The PES curvature also determines the shear modulus [32,39]

$$C_{44} = \frac{d}{\sigma}\frac{\partial^2 U}{\partial x'^2} = \frac{16\pi^2 d}{\sqrt{3}a^4}U_{\text{eff}}, \tag{5}$$

where $\sigma = \sqrt{3}a^2/4$ is the area per carbon atom and $d = 3.46$ Å is the interlayer distance. The shear moduli estimated for different moiré patterns do not exceed 0.4 GPa (Table II). This is an order of magnitude smaller than the DFT result for the coaligned graphene bilayer of 3.8–4.1 GPa [52] because the shear modulus is proportional to $\Delta U N_c$.

The PES also determines the static friction force f_{s} for moving the layers as a whole, i.e., the maximal first derivative of the potential energy along the minimum energy path (MEP) between adjacent energy minima and, correspondingly, the shear strength τ related to it as $\tau = f_{\text{s}}/\sigma$ (here the force is taken per atom of the upper layer). Analogous estimates of shear strength have been performed first for commensurate double-walled nanotubes [55]. For $U_1 > 0$, the MEP between

adjacent energy minima corresponds to the line $x' = 0$ and y' from $a/\sqrt{3N_c}$ to $2a/\sqrt{3N_c}$ in Eq. (3). The force along the MEP is given by

$$-\frac{\partial U}{\partial y'}\bigg|_{x'=0} = 2k'_y U_1(\sin(k'_y y') + \sin(2k'_y y')), \qquad (6)$$

and the force extrema are determined by the equation $\cos(k'_y y') + 2\cos(2k'_y y') = 0$. The latter equation gives that the maximal absolute force is achieved for $\cos(k'_y y') = -(1 + \sqrt{33})/8$ for the considered MEP. From this, we find that the shear strength is $\tau = 6.183\sqrt{N_c}U_1/a^3$ for $U_1 > 0$.

For $U_1 < 0$, the MEP corresponds to $y' = 0$ and x' from 0 to $a/\sqrt{N_c}$ in Eq. (3). In this case,

$$-\frac{\partial U}{\partial x'}\bigg|_{y'=0} = 2k'_x U_1 \sin(k'_x x'). \qquad (7)$$

The maximal absolute force is achieved for $x' = a/4$. Correspondingly, the shear strength is $\tau = 16\pi\sqrt{N_c}U_1/\sqrt{3}a^3$.

The shear strength τ values estimated for different moiré patterns are within 0.02 GPa (Table II). From typical DFT values for the amplitude of PES corrugations for coaligned graphene layers of about 15 meV per atom of the upper layer [35,52], we deduce that the shear strength in that case should be about 0.22 GPa, i.e., an order of magnitude greater. As seen from the above equations, the shear strength for moiré patterns is proportional to $\sqrt{N_c}\Delta U$.

When the graphene layers are rotated with respect to each other by an arbitrary angle that does not correspond to any commensurate moiré pattern, the area contribution to the PES vanishes, and the PES of an infinite incommensurate twisted bilayer becomes flat. Therefore the interaction energy in such a fully incommensurate state can be found as an average over the PES: $U_{rot} = \langle U \rangle_{x,y}$ [32,35,39,43]. The barrier ΔU_{rot} for relative rotation of the layers to a fully incommensurate state can thus be obtained by subtracting the energy in the minimum from U_{rot}. From Eq. (3), one gets $\Delta U_{rot} = 1.5U_1$ for $U_1 > 0$ and $-3U_1$ for $U_1 < 0$. The values of the barrier estimated for the moiré patterns considered are within 0.06 meV per atom of the upper layer (Table II). Obviously, they are much smaller than the previous predictions for the coaligned graphene bilayer of 4 meV/atom [56,57] and 5 meV/atom [35].

Structural superlubricity can be lost via rotation of the layers with the same lattice constant to the commensurate ground state with coaligned layers [1,4–7,9,11–13,58]. Robust superlubricity has been recently achieved for systems with a lattice mismatch such as heterostructures composed of layers of different 2D materials [20] or layers of the same 2D material under different applied tensions [13,17]. For such robust superlubric systems, the relative rotation of the layers to a commensurate interface with the loss of superlubricity is not possible. Here we propose that robust superlubricity can also be achieved for systems in which rotation of the layers to the commensurate ground state with coaligned layers is possible but hindered by a barrier. For twisted commensurate layers, such a rotation should occur through a fully incommensurate state. Although the barriers between the local minimum of a twisted commensurate state and a fully incommensurate state calculated here are rather small, they might be sufficient to prevent the relative rotation of layers for a sufficiently large contact area and thus ensure robust macroscopic superlubricity. Further macroscale investigations would be needed to confirm this hypothesis.

It should be kept in mind that the values of the physical quantities obtained in this section and listed in Table II are based on calculations with the Kolmogorov-Crespi potential [49] but its adequacy for twisted graphene layers has not been proven. Nevertheless, the potential gives a reasonable dependence of the amplitude ΔU of PES corrugations on the size of the unit cell of the moiré pattern [Fig. 2(f)] and thus should properly describe the trend in the evaluated physical quantities for different moiré patterns. Once a more reliable potential for twisted graphene layers is available, it can be used to obtain more accurate estimates based on the equations given above. On the other hand, as soon as any of these physical quantities is accessed experimentally (by analogy with the measurements for coaligned graphene layers [53,54]), classical potentials can be refined to improve the description of the PES of the twisted layers on the basis of the above formalism. We also believe that the simple shape of the PES can be a universal property for commensurate twisted bilayers consisting of diverse 2D materials. This means that physical properties of moiré patterns of other 2D materials can be estimated in a similar way.

The results of the geometrical analysis presented here are derived without taking into account structural relaxation. Our calculations show that accounting for structural relaxation does not lead to changes in the shape of the PES and it is still described by the first Fourier harmonics (whereas some increase in the amplitude ΔU of PES corrugations occurs). Thus all the equations presented here are still valid. The influence of structural relaxation on structural and tribological properties of commensurate moiré patterns will be considered elsewhere.

IV. DISCUSSION AND CONCLUSIONS

PESs of the interlayer interaction have been calculated for a set of commensurate moiré patterns of twisted graphene bilayer using the registry-dependent Kolmogorov-Crespi potential. The amplitude of PES corrugations is found to exceed the calculation accuracy only for five moiré patterns with the smaller unit cell sizes. All calculated PESs have the same simple shape which corresponds to the symmetry of commensurate moiré patterns, and the size of the unit cell of the PESs is inversely related to the unit cell size of the moiré pattern. The amplitude of PES corrugations exponentially decreases with increasing unit cell size of the moiré pattern. An analytical expression which is based on the first Fourier harmonics describing the PES has been derived. The calculated PESs can be approximated by the derived expression with an accuracy within 1% relative to the amplitude of PES corrugations. Since the derived expression contains a single energetic parameter, it has been used to estimate a set of physical quantities determined by the PES such as the shear mode frequency, the shear modulus, the shear strength, and the barrier for relative rotation of the commensurate twisted layers to a fully incommensurate state. We propose that the latter barrier might prevent the rotation of the layers from the

twisted commensurate state to the ground commensurate state through a fully incommensurate state and therefore can possibly lead to robust macroscopic superlubricity for a sufficiently large contact area.

Not only can the approximation by the first Fourier harmonics be applied for consideration of the interlayer interaction energy, but also, for example, such an approximation for coaligned layers was used for the analysis of electronic properties of twisted graphene [51] and a graphene/h-BN heterostructure [41,51]. Moreover, since the approximation of the PES of the interlayer interaction by the first Fourier harmonics is a universal property for coaligned layers of diverse 2D materials [32], we believe that the simple shape of the PES obtained here for a twisted commensurate graphene bilayer can also be universal for any commensurate moiré patterns consisting of layers of diverse 2D materials.

The raw data for the calculated PESs required to reproduce our findings are available to download [59].

[1] M. Hirano and K. Shinjo, Phys. Rev. B **41**, 11837 (1990).

[2] M. Hirano, K. Shinjo, R. Kaneko, and Y. Murata, Phys. Rev. Lett. **67**, 2642 (1991).

[3] O. Hod, E. Meyer, Q. Zheng, and M. Urbakh, Nature (London) **563**, 485 (2018).

[4] G. S. Verhoeven, M. Dienwiebel, and J. W. M. Frenken, Phys. Rev. B **70**, 165418 (2004).

[5] M. Dienwiebel, N. Pradeep, G. S. Verhoeven, H. W. Zandbergen, and J. W. M. Frenken, Surf. Sci. **576**, 197 (2005).

[6] A. E. Filippov, M. Dienwiebel, J. W. M. Frenken, J. Klafter, and M. Urbakh, Phys. Rev. Lett. **100**, 046102 (2008).

[7] Z. Xu, X. Li, B. I. Yakobson, and F. Ding, Nanoscale **5**, 6736 (2013).

[8] E. Koren and U. Duerig, Phys. Rev. B **94**, 045401 (2016).

[9] F. Bonelli, N. Manini, E. Cadelano, and L. Colombo, Eur. Phys. J. B **70**, 449 (2009).

[10] M. M. van Wijk, M. Dienwiebel, J. W. M. Frenken, and A. Fasolino, Phys. Rev. B **88**, 235423 (2013).

[11] Y. Guo, W. Guo, and C. Chen, Phys. Rev. B **76**, 155429 (2007).

[12] Y. Shibuta and J. A. Elliott, Chem. Phys. Lett. **512**, 146 (2011).

[13] K. Wang, W. Ouyang, W. Cao, M. Ma, and Q. Zheng, Nanoscale **11**, 2186 (2019).

[14] H. Zhang, Z. Guo, H. Gao, and T. Chang, Carbon **94**, 60 (2015).

[15] H. Zhang and T. Chang, Nanoscale **10**, 2447 (2018).

[16] H. Zhang, J. Qu, Z. Guo, L. Huang, and Q. Xie, AIP Adv. **12**, 115312 (2022).

[17] C. Androulidakis, E. N. Koukaras, G. Paterakis, G. Trakakis, and C. Galiotis, Nat. Commun. **11**, 1595 (2020).

[18] Z. Liu, J. Yang, F. Grey, J. Z. Liu, Y. Liu, Y. Wang, Y. Yang, Y. Cheng, and Q. Zheng, Phys. Rev. Lett. **108**, 205503 (2012).

[19] C. C. Vu, S. Zhang, M. Urbakh, Q. Li, Q.-C. He, and Q. Zheng, Phys. Rev. B **94**, 081405(R) (2016).

[20] Y. Song, D. Mandelli, O. Hod, M. Urbakh, M. Ma, and Q. Zheng, Nat. Mater. **17**, 894 (2018).

[21] D. Mandelli, I. Leven, O. Hod, and M. Urbakh, Sci. Rep. **7**, 10851 (2017).

[22] A. S. Minkin, I. V. Lebedeva, A. M. Popov, and A. A. Knizhnik, Phys. Rev. B **104**, 075444 (2021).

[23] A. S. Minkin, I. V. Lebedeva, A. M. Popov, and A. A. Knizhnik, Nanotechnol. Russ. **17**, 472 (2022).

[24] J. M. Campanera, G. Savini, I. Suarez-Martinez, and M. I. Heggie, Phys. Rev. B **75**, 235449 (2007).

[25] I. V. Lebedeva and A. M. Popov, J. Phys. Chem. C **124**, 2120 (2020).

[26] A. M. Popov, I. V. Lebedeva, A. A. Knizhnik, Y. E. Lozovik, and B. V. Potapkin, Phys. Rev. B **84**, 045404 (2011).

[27] E. J. Mele, J. Phys. D: Appl. Phys. **45**, 154004 (2012).

[28] T. Kabengele and E. R. Johnson, Nanoscale **13**, 14399 (2021).

[29] A. N. Kolmogorov and V. H. Crespi, Phys. Rev. Lett. **85**, 4727 (2000).

[30] A. V. Belikov, Y. E. Lozovik, A. G. Nikolaev, and A. M. Popov, Chem. Phys. Lett. **385**, 72 (2004).

[31] E. Bichoutskaia, M. I. Heggie, A. M. Popov, and Y. E. Lozovik, Phys. Rev. B **73**, 045435 (2006).

[32] A. V. Lebedev, I. V. Lebedeva, A. M. Popov, A. A. Knizhnik, N. A. Poklonski, and S. A. Vyrko, Phys. Rev. B **102**, 045418 (2020).

[33] O. V. Ershova, T. C. Lillestolen, and E. Bichoutskaia, Phys. Chem. Chem. Phys. **12**, 6483 (2010).

[34] I. V. Lebedeva, A. A. Knizhnik, A. M. Popov, Y. E. Lozovik, and B. V. Potapkin, Phys. Chem. Chem. Phys. **13**, 5687 (2011).

[35] A. M. Popov, I. V. Lebedeva, A. A. Knizhnik, Y. E. Lozovik, and B. V. Potapkin, Chem. Phys. Lett. **536**, 82 (2012).

[36] I. V. Lebedeva, A. A. Knizhnik, A. M. Popov, Y. E. Lozovik, and B. V. Potapkin, Phys. E (Amsterdam) **44**, 949 (2012).

[37] S. Zhou, J. Han, S. Dai, J. Sun, and D. J. Srolovitz, Phys. Rev. B **92**, 155438 (2015).

[38] M. Reguzzoni, A. Fasolino, E. Molinari, and M. C. Righi, Phys. Rev. B **86**, 245434 (2012).

[39] A. V. Lebedev, I. V. Lebedeva, A. A. Knizhnik, and A. M. Popov, RSC Adv. **6**, 6423 (2016).

[40] A. M. Popov, I. V. Lebedeva, A. A. Knizhnik, Y. E. Lozovik, B. V. Potapkin, N. A. Poklonski, A. I. Siahlo, and S. A. Vyrko, J. Chem. Phys. **139**, 154705 (2013).

[41] J. Jung, A. M. DaSilva, A. H. MacDonald, and S. Adam, Nat. Commun. **6**, 6308 (2015).

[42] H. Kumar, D. Er, L. Dong, J. Li, and V. B. Shenoy, Sci. Rep. **5**, 10872 (2015).

[43] A. V. Lebedev, I. V. Lebedeva, A. M. Popov, and A. A. Knizhnik, Phys. Rev. B **96**, 085432 (2017).

[44] T. Vuković, M. Damnjanović, and I. Milošević, Phys. E **16**, 259 (2003).

[45] E. Bichoutskaia, A. M. Popov, A. El-Barbary, M. I. Heggie, and Y. E. Lozovik, Phys. Rev. B **71**, 113403 (2005).

[46] E. Bichoutskaia, A. M. Popov, Y. E. Lozovik, O. V. Ershova, I. V. Lebedeva, and A. A. Knizhnik, Phys. Rev. B **80**, 165427 (2009).

[47] A. M. Popov, Y. E. Lozovik, A. S. Sobennikov, and A. A. Knizhnik, J. Exp. Theor. Phys. **108**, 621 (2009).

[48] A. M. Popov, I. V. Lebedeva, and A. A. Knizhnik, Appl. Phys. Lett. **100**, 173101 (2012).

[49] A. N. Kolmogorov and V. H. Crespi, Phys. Rev. B **71**, 235415 (2005).

[50] See Supplemental Material at http://link.aps.org/supplemental/ 10.1103/PhysRevB.108.085411 for details of the Kolmogorov-Crespi and Lebedeva potentials and the PESs for the moiré patterns with the amplitude of the PES corrugations lower than the artifacts related with the finite value of the cutoff radius of the potential.

[51] J. Jung, A. Raoux, Z. Qiao, and A. H. MacDonald, Phys. Rev. B **89**, 205414 (2014).

[52] I. V. Lebedeva, A. V. Lebedev, A. M. Popov, and A. A. Knizhnik, Comput. Mater. Sci. **128**, 45 (2017).

[53] D. Boschetto, L. Malard, C. H. Lui, K. F. Mak, Z. Li, H. Yan, and T. F. Heinz, Nano Lett. **13**, 4620 (2013).

[54] P. H. Tan, W. P. Han, W. J. Zhao, Z. H. Wu, K. Chang, H. Wang, Y. F. Wang, N. Bonini, N. Marzari, N. Pugno, G. Savini, A. Lombardo, and A. C. Ferrari, Nat. Mater. **11**, 294 (2012).

[55] E. Bichoutskaia, O. V. Ershova, Y. E. Lozovik, and A. M. Popov, Tech. Phys. Lett. **35**, 666 (2009).

[56] I. V. Lebedeva, A. A. Knizhnik, A. M. Popov, O. V. Ershova, Y. E. Lozovik, and B. V. Potapkin, Phys. Rev. B **82**, 155460 (2010).

[57] I. V. Lebedeva, A. A. Knizhnik, A. M. Popov, O. V. Ershova, Y. E. Lozovik, and B. Potapkin, J. Chem. Phys. **134**, 104505 (2011).

[58] X. Feng, S. Kwon, J. Y. Park, and M. Salmeron, ACS Nano **7**, 1718 (2013).

[59] A. S. Minkin, I. V. Lebedeva, A. M. Popov, S. A. Vyrko, N. A. Poklonski, and Y. E. Lozovik, Data for: Interlayer interaction, shear vibrational mode, and tribological properties of two-dimensional bilayers with a commensurate moiré pattern, Mendeley Data, 2023, doi: 10.17632/svnpzbjc3t.

[60] https://rscf.ru/en/project/23-42-10010/.

[61] http://ckp.nrcki.ru.